INTERNATIONAL JOURNAL OF HYDROGEN ENERGY 44 (2019) 1239–1252

Available online at www.sciencedirect.com

ScienceDirect

journal homepage: www.elsevier.com/locate/he

Comparative analysis of H_2-diesel co-combustion in a single cylinder engine and a chassis dynamometer vehicle

Midhat Talibi [a,*], *Paul Hellier* [a], *Martin Watkinson* [b], *Nicos Ladommatos* [a]

[a] *Department of Mechanical Engineering, University College London, Torrington Place, London, WC1E 7JE, UK*
[b] *HORIBA MIRA Ltd., Watling Street, Nuneaton, Warwickshire, CV10 0TU, UK*

ARTICLE INFO

Article history:
Received 27 June 2018
Received in revised form
5 November 2018
Accepted 10 November 2018
Available online 10 December 2018

Keywords:
Combustion
Hydrogen
Emissions
Particulates
Chassis dynamometer
EGR

ABSTRACT

Concerns as to the adverse effects of diesel engine exhaust on urban air quality have resulted in increasingly stringent emissions legislation, with the prospect of many major global cities potentially banning diesel vehicles. Emissions of nitrogen oxides (NO_x) and particulate matter (PM) are linked to increases in premature mortality, and the simultaneous control of both pollutants through modified combustion strategies presents a significant challenge. In this work, the effects of displacing diesel fuel with hydrogen on exhaust emissions were investigated in both a single cylinder research engine and in a demonstration vehicle. In the initial stage, tests were undertaken on a supercharged, direct injection, single cylinder diesel research engine at different engine loads, intake air pressures and EGR levels. Hydrogen was aspirated with the intake air, and EGR was simulated by supplying the intake pipe with compressed nitrogen gas. The results showed a reduction in CO_2 and particulate emissions with increasing H_2 addition, and an increase in NO_x emissions at H_2 levels greater than 10% of the total input energy to the engine. The next stage involved tests on a chassis dynamometer with a small van equipped with the multi-cylinder version of the single cylinder research engine. The van was fitted with a programmable H_2 augmentation system, with H_2 addition levels specified by accelerator pedal position. During full drive cycle tests conducted with and without H_2 augmentation up to 10%, an average rate of 1 kW of H_2 was supplied to the engine. With H_2 augmentation, over the total drive-cycle, reductions in CO, NO_x and particle number were observed, but a higher total PM mass was recorded.

Introduction

Concurrent to increasingly stringent legislation restricting levels of toxic pollutants permitted in exhaust gases from internal combustion engines utilised for road transport [1], there has been growing public awareness and concern as to the detrimental impact of such emissions on human health, especially in urban areas. In the UK, 29,000 premature deaths per year have been attributed to anthropogenic emissions of particulate matter (PM) [2], with 3000 of these in London alone. Similarly, levels of atmospheric nitrogen dioxide (NO_2) as measured in 2010 are estimated to be responsible for approximately 5800 premature deaths per year in London [3].

* *Corresponding author.*
E-mail address: m.talibi@ucl.ac.uk (M. Talibi).
https://doi.org/10.1016/j.ijhydene.2018.11.092

While emissions of both PM and nitrogen oxides (NO_x) arise from a range of anthropogenic combustion activities, it is diesel engine powered vehicles that both policy makers and the mainstream media have focused on in recent years as a significant contributor to emissions of both [4]. With the added realisation of the discrepancies between results of legislative exhaust emissions tests and 'real-world' emission levels [5], several major cities worldwide have announced plans to ban diesel powered vehicles in the next 15–20 years [6,7]. However, regardless of the future uptake of zero emission thermal and electric powertrains so as to address these concerns, there will likely remain a great number of older existing diesel fuel powered vehicles in use, with 1.28 million and 1.06 million new diesel passenger cars registered in the UK alone in 2016 and 2017 respectively [8].

Many modern diesel passenger cars and light goods vehicles benefit from advanced exhaust after-treatment devices which are able to significantly reduce tailpipe-out emissions of both NOx and PM [9,10]. However, the successful implementation of such devices on older vehicles can be complex and might result in insufficient reductions in pollutant species to allow these vehicles to enter new ultra-low emission zones, such as those intended to be in operation in London by 2020 [11]. An additional approach to the reduction of diesel engine exhaust emissions that has received significant attention is the co-combustion of gaseous and liquid fuels, for example varying proportions of methane and hydrogen (H_2) [12], LPG reformate products [13], Brown's gas [14,15], and intake aspirated and vaporised short chain alcohols [16], and has been the subject of several review papers [17,18]. The displacement of diesel fuel with hydrogen has received particular attention given the inherent potential for reduction of carbon derived exhaust pollutants, including direct injection light-duty engines, with previous investigations of effects on exhaust emissions [19] and the impact of H_2 on the formation of NOx and PM utilising in-cylinder sampling [20], in conjunction with biodiesel combustion [21–24], and also in heavy duty diesel engines [25–29]. Various options for the provision of H_2 on-board vehicle for this purpose have been suggested, including electrolysis of water [26] and catalytic reforming of diesel fuel utilising energy recovered from engine exhaust, as suggested in the context of heavy duty diesel engines by Morgan et al. [30] and with the addition of water to the reformation process for increased H_2 production by Tsolakis et al. [31]. A further option is the storage of hydrogen as a solid in the form of hydrides which release gaseous H_2 on heating [32–35]. Diesel engine tests of fuels containing dissolved sodium borohydride by Hellier et al. [36] found the presence of the hydride within the fuel to impede injector function, however, systems utilising on-board storage of solid hydride materials for provision of up to 20 KW of energy from H_2 for automotive applications are now being commercially developed [37].

Several previous studies of hydrogen diesel co-combustion in which reductions in PM emissions have been achieved, due to the reduction in intake fuel carbon, have also noted increases in exhaust NOx emissions with increasing concentrations of H_2 [20,38–40]. However, where emission control techniques, in particular exhaust gas recirculation (EGR), and conditions representative of modern diesel engines, such as intake air boosting, have been utilised during engine tests of hydrogen diesel co-combustion, reductions of PM levels without concurrent NOx increases have been reported [24,28,30,41–45]. For example, Shin et al. [41] utilised cooled and heavy EGR to control NO_x emissions from a H_2 co-fuelled diesel engine and observed that at an EGR ratio of 31%, and when the supplied H_2 was equivalent to 10% of the total intake lower heating valve, the specific NO_x emissions reduced by 10%. Talibi et al. [42] observed that up to 10% by energy content of diesel fuel could be replaced with intake aspirated H_2 in a single cylinder diesel engine without an increase in exhaust NOx emissions. Roy et al. [44] used charge dilution with N_2 gas to reduce NO_x emissions and allow a higher energy contribution from H_2 without H_2 autoignition prior to diesel pilot ignition in a H_2 fuelled, supercharged engine. The authors managed to attain approximately 90% H_2 energy contribution with the engine producing almost no smoke, 5 ppm of CO, 15 ppm of unburned THC and operating at a brake thermal efficiency of 42% [44]. In tests with a heavy duty CI engine in which H_2 was injected into the intake manifold at levels up to 98% of the total energy supplied to the engine, Dimitriou et al. [45] found that use of EGR with H_2 addition only achieved simultaneous reductions in both NOx and PM at low load engine operating conditions, with increased combustion temperatures arising from H_2 resulting in significantly higher NOx emissions where EGR was not applied.

While the potential benefits of hydrogen diesel co-combustion for control of engine exhaust emissions have been observed in engine dynamometer tests, such experiments have, in the main, been undertaken at steady state conditions with considerable engine warm-up periods and precise control of variables such as speed and load. For the displacement of fossil diesel fuel with hydrogen to make a meaningful contribution to the control of pollutant emissions from diesel powered vehicles, there is a need for validation of these observations at transient engine conditions representative of on-road driving conditions. This paper therefore presents results of experiments investigating the effects of displacing diesel fuel with intake aspirated H_2 on exhaust emissions in a single cylinder research diesel engine operating with intake boosting and simulated EGR at a range of engine loads, and from chassis dynamometer vehicle tests operating on an urban drive cycle.

Experimental setup

The hydrogen-diesel fuel co-combustion tests were carried out at two different experimental facilities, a single cylinder diesel research engine facility at UCL and a demonstration vehicle (with a multi-cylinder version of the single cylinder engine) on a chassis dynamometer at HORIBA MIRA Ltd.

Single cylinder research engine

At UCL, co-combustion tests were conducted on a four-stroke, water cooled, single cylinder diesel engine described previously by the authors [42,46], consisting of a 2.0 L, 4-cylinder Ford Duratorq cylinder head (including valves, piston and connecting rod) mounted on a single cylinder Ricardo Hydra crankcase - Table 1 lists the engine geometry and other

specifications of the test setup. For the derivation of heat release rate (utilising a one-dimensional thermodynamic model) and indicated mean effective pressures (IMEP), the engine in-cylinder gas pressure was acquired, to a resolution of 0.2 CAD, using a piezoelectric pressure transducer (Kistler 6056A) coupled to a charge amplifier (Kistler 5018). The measured in-cylinder pressure was pegged to the inlet manifold pressure at the piston BDC position every engine cycle. Various other operational pressures and temperatures were also monitored during the engine experiments and logged on PCs using National Instruments (NI) data acquisition systems. A six-hole, servo-hydraulic solenoid valve fuel injector was used for direct injection of diesel fuel, with the injection pressure (±1 bar), injection timing (±0.1 CAD) and duration of injection (±1 μs) controlled using a custom ECU (EmTronix EC-GEN500). H_2 was supplied from a compressed gas cylinder and fed into the engine intake manifold 350 mm upstream of the intake valves to be aspirated into the combustion chamber with the intake air. The flow of H_2 (measured in normal l/min) was metered using a thermal mass flow controller (Bronkhorst F-201AV-70K, accuracy ±0.08 l/min), and a flash back arrestor and a non-return valve were installed in the H_2 supply line for safety. In-order to simulate EGR-like conditions in the engine by reducing the amount of O_2 in the intake charge, N_2 gas was also fed in the intake manifold, via a separate mass flow controller, Bronkhorst F-202AV-70K (accuracy ±0.15 l/min).

The intake air pressure was boosted using a supercharger system, to create in-cylinder conditions that matched a turbocharged engine. The system consisted of a rotary screw supercharger (Eaton M45), connected to an electric motor via a drive belt, with the speed of the motor controlled by means of a thyristor drive. A heat exchanger was installed downstream of the supercharger to control the intake air temperature, while a positive displacement volumetric air-flow meter (Romet G65) was mounted upstream of the supercharger to measure the air flow rate. The pressure in the intake air manifold was measured 160 mm upstream of the inlet valves using a piezoresistive transducer.

The exhaust gas emissions were measured using an automotive gas analyser rack (Horiba MEXA-9100HEGR) which housed the following analysers; chemiluminescence analyser for NOx determination, flame ionization detector for analysing levels of THC, non-dispersive infrared absorption analyser for measurement of CO and CO_2, and a magneto-pneumatic analyser for O_2 concentrations. Additionally, the number and size distribution of exhaust gas particulates was determined using a differential mobility spectrometer (Cambustion DMS500). Exhaust gas samples were collected 300 mm downstream of the exhaust valves and conveyed to the analysers via heated lines, which were maintained at 190 °C and 80 °C for the measurement of gaseous and particulate emissions, respectively. Fig. 1 shows a schematic of the single cylinder engine test facility, including the supercharger system and intake gas delivery setup.

Table 1 – Specifications of the single cylinder engine.

Cylinder bore	86 mm
Crankshaft stroke	86 mm
Swept volume	499.56 cm^3
Compression ratio (geometric)	18.3: 1
Maximum in-cylinder pressure	150 bar
Piston design	Central ω – bowl in piston
Fuel injection pump	Delphi single-cam radial-piston pump
High pressure common rail	Delphi solenoid controlled, 1600 bar max.
Diesel fuel injector	Delphi DFI 1.3 6-hole solenoid valve injector
Electronic fuel injection system	1 μs duration control
Crank shaft encoder	1800 ppr, 0.2 CAD resolution

Chassis dynamometer multi-cylinder vehicle

At Horiba MIRA Ltd., subsequent H_2-diesel co-combustion experiments were undertaken with a vehicle mounted on a chassis dynamometer in the Vehicle Exhaust Emissions Laboratory (VEEL). A 2004 Ford Transit 2.0 Duratorq DI diesel van with EGR was utilised for the chassis dynamometer tests, as it had the same head as the single-cylinder research engine at UCL. Modifications to the vehicle for supply of H_2 to the engine intake manifold were kept to a minimum, to be representative of a H_2 delivery system that could be retrofitted to a wide range of vehicle makes and models. The H_2 flow rate to the manifold was based on the accelerator pedal position so that the volume of H_2 supplied at any given time could be matched to the engine output load. A replacement accelerator pedal unit was installed on the vehicle and modified to give parallel high impedance output signals for the new H_2 controller unit, without interfering with the base vehicle signals to/from the ECU; hence, no changes to the engine ECU were required. The output from the modified pedal unit was sent to a signal conditioning and analysis micro-processor in the H_2 controller. The pedal position was verified against an internal map (profile of H_2 flow against pedal position) to ascertain the desired H_2 demand, which was then fed to the H_2 mass flow controller via CAN communications protocol. The controller unit also checked for faulty signals from the pedal output, and took corrective measures (such as, switching off H_2 flow) if the pedal position signal was outside a pre-determined safe range. System signal conditioning, validation, and mapping with communications was developed and simulated using auto-coding tools for rapid development and versatility to changing requirements, for example, re-mapping of the H_2 demand profile.

Exhaust gas emissions were measured using a Horiba MEXA-7500DEGR analyser rack, which housed detectors for the measurement of CO, CO_2, unburned THC and NO_x. The gaseous exhaust emissions were collected in sampling bags from the vehicle prior to analysis by the analyser rack. Due to the capacity of each bag, the emissions were collected in 4 separate bags over the duration of each test. The number of particles in the exhaust were measured with a Horiba MEXA-2200SPCS, which was connected directly to the vehicle exhaust via a dilution tunnel. The instrument utilised the laser scattering condensation particle counting technique, and specified a counting efficiency of greater than 90% for particles larger than 41 nm and about 50% for particles between 23 nm and 41 nm diameter. This same efficiency profile was applied in post processing to particle size distribution results from the particulate spectrometer (DMS500) at UCL, to allow for a more accurate comparison of particulate results

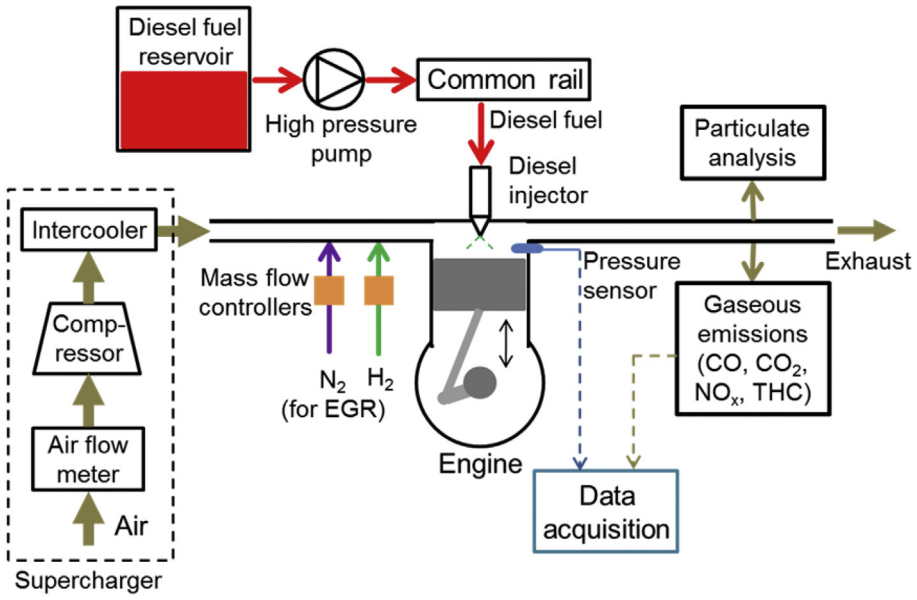

Fig. 1 – Schematic showing test engine arrangement including the super charger system and exhaust emissions instrumentation.

from both experimental setups. In addition, the exhaust particle mass was also measured by collecting exhaust particles on a glass fibre filter paper for the duration of each test. The gas and particle samples were collected upstream of the vehicle after-treatment systems to allow for comparison with the single cylinder engine, which does not have any after-treatment systems installed. Fig. 2 shows a schematic of the test setup, while Table 2 lists some specification of the demonstration vehicle.

Experimental methodology

Single cylinder engine tests

For the single cylinder engine tests, the engine speed, the diesel fuel injection pressure and diesel fuel injection timing were kept constant at 1200 rpm, 900 bar and 6 CAD BTDC respectively. The fuel injection timing of 6 CAD BTDC was optimised for maximum IMEP for the diesel only tests, and was fixed so that the effect of H_2 addition on the ignition delay of the in-cylinder charge could be observed. Throughout this work, the ignition delay has been defined as the time in crank angle degrees (CAD) between the start of the injection signal supplied to the diesel fuel injector (SOI) and the start of combustion (SOC) as indicated by the first incidence of positive heat release. The fossil diesel fuel had zero FAME (fatty acid methyl ester) content, a carbon to hydrogen mass ratio of 6.32:1 and cetane number of 53.2. Compressed H_2 gas of purity 99.995% and compressed N_2 gas of purity 99.5% were obtained from a commercial gas supplier (BOC).

Table 3 summarises the conditions used for these tests showing the various engine load, intake air boost and EGR combinations – for each test, the amount of diesel fuel was incrementally reduced and replaced by H_2 in sufficient quantities to maintain a constant engine load (IMEP). A wide range of engine loads were tested on the single cylinder engine ranging from 4 bar to 11.5 bar IMEP). For the three lowest loads, 4, 5.5 and 7 bar IMEP, the engine was run in a naturally aspirated condition. For the three highest loads, intake air boost and EGR was applied, as described in Table 3. As mentioned earlier, N_2 gas was used to simulate EGR-like conditions in the engine, where the measured flow rates of N_2 gas and intake air were used to determine the reduction in O_2 (v/v) in the intake air because of the aspirated N_2. It is pertinent to mention here that the aspirated H_2 also displaced intake air, and therefore, the flow rates of both H_2 and N_2 were taken into account when calculating the reduction in intake O_2. The temperature of the gas mixture in the engine intake manifold was kept at 30 ± 1 °C

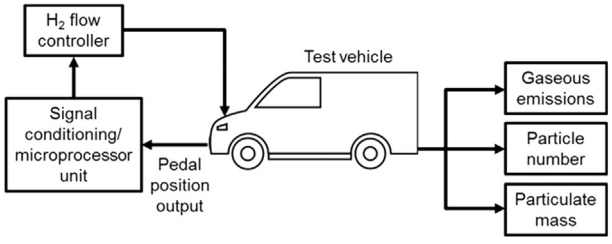

Fig. 2 – Schematic of the demonstration vehicle test facility.

Table 2 – Specifications of the chassis dynamometer test vehicle.

Vehicle (make, model)	Ford Transit Duratorq 2.0 DI
Transmission	5 gear Manual
Inertial weight	1930 kg
Tyre size	195/70 R15
Tyre pressure	4 bar
Oil temperature	80 °C
Coolant temperature	80 °C

Table 3 – Test operating condition matrix showing different intake air boost-engine load combinations at various EGR ratios and engine speed of 1200 rpm, for a constant intake temperature of 30 °C in the engine intake manifold.

Engine load (bar IMEP)	Indicated engine power (kW)	Intake air boost pressure (bar)	% points O_2 reduction (v/v)
4	2.00	–	–
5.5	2.75	–	–
7	3.50	–	–
8.5	4.25	1.33	1
10	5.00	1.67	1
11.5	5.75	1.99	1

Table 4 – Densities and lower heating values of diesel fuel and hydrogen at 1 atm and 300 K [14].

Property	Density (kg/m^3)	Lower heating value (MJ/kg)
Diesel fuel	831.9	43.14
Hydrogen	0.0838	120

for all the tests, measured 200 mm upstream of the inlet valve. It should also be noted that the corresponding engine power (kW) for each engine load shown in Table 3 is for the half-litre single cylinder engine used in these tests, and has not been scaled for the 2-L, 4-cylinder version of the engine. Table 4 shows the density and lower heating values of the diesel fuel and H_2 gas utilised in these experiments [47]. Fig. 3 shows the percentage ratio of the energy supplied to the engine from H_2 relative to the total energy supplied (diesel fuel plus H_2); also shown are the corresponding power content (Fig. 3a) and flow rates (Fig. 3b) of H_2 supplied to the engine.

Chassis dynamometer vehicle tests

The vehicle on the chassis dynamometer was driven on the PCO-Cenex TfL Taxi Cycle. This drive cycle has been co-developed by Transport for London's Public Carriage Office (TfL PCO), which regulates London's taxi and private hire services, and Cenex, UK's first Centre of Excellence for low carbon technologies in automotive applications, and is considered to be representative of driving conditions for diesel powered vehicles in urban cities. Fig. 4 shows the vehicle speed profile for the drive cycle. The 48-min cycle forms a three-phase test plus 3 min and 12 s of engine off time between phases 1 and 2. Each phase represents one of the three London zones, Central, Inner and Outer. Phase 3 has been weighed by a factor of 0.65 to retain correct proportionality of a working day.

As described in Section 2.2 earlier, the supply of H_2 to the intake manifold of the test vehicle was based on the accelerator pedal position. Based on tests undertaken on the single cylinder engine (discussed later in Section 4.1), a profile for H_2 flow against pedal position was defined and applied to the flow controller unit, and is shown in Fig. 5 – the figure also shows the actual mass flow rate supplied to the engine as measured by the H_2 flow controller. The profile was based on a maximum of 10% H_2 augmentation of energy from diesel fuel. The value of 10% was selected as a potentially optimised condition that would significantly reduce PM emissions from the vehicle, based on the UCL single cylinder engine tests (presented in Section 4.1). The maximum defined H_2 flow rate of 0.5 l/sec (30 l/min) is equivalent to approximately 4 kW of applied H_2 energy at 10% augmentation of diesel fuel. Fig. 6a shows the expected H_2 flow rate to the vehicle intake manifold during a portion of the PCO-Cenex TfL drive cycle. It was calculated that 371 L of H_2 was required over the entire drive cycle (average flow rate = 7.5 l/min), which equates to an average H_2 power demand rate of approximately 1 kW over the whole cycle. Fig. 6b also shows the pedal position for the same portion of the drive cycle. It can be seen from this figure that the H_2 flow is very responsive to the change in pedal position, in that after H_2 addition there is an easing off of the throttle pedal due to the immediate change in engine speed (corresponding to an increasing in engine power).

Results and discussion

Single cylinder engine tests

Fig. 7a shows the apparent net heat release rate curves for two engine loads, 4 bar and 7 bar IMEP, for different H_2 levels. Fig. 7b also shows heat release rate curves, but for higher loads of 8.5 bar and 10 bar IMEP, and with intake air boosting (1.33 bar and 1.67 bar) and a constant 1% reduction in intake O_2 level. The heat release rate was derived from the measured in-cylinder gas pressure utilising a one dimensional and single

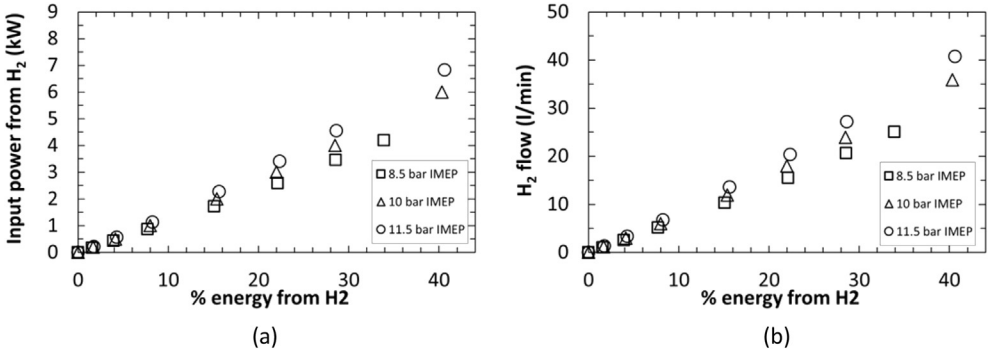

Fig. 3 – (a) Power content of H_2 (kW) and (b) H_2 flow rates (l/min) at constant engine loads and varying percentage energy from H_2.

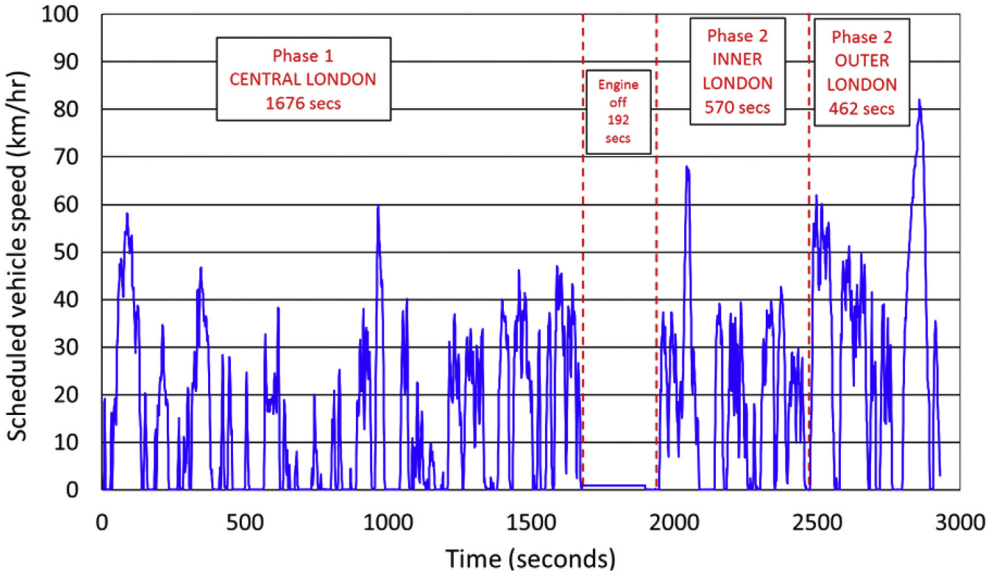

Fig. 4 – PCO-Cenex TfL Taxi drive cycle profile.

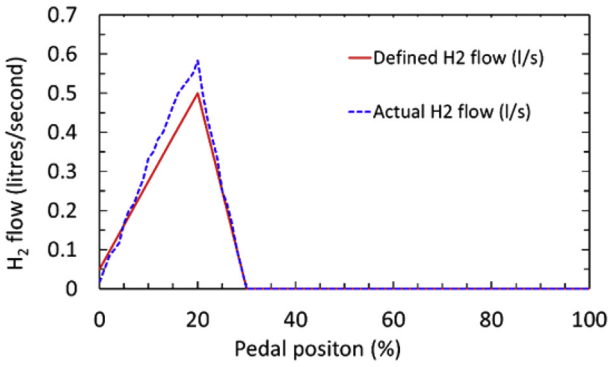

Fig. 5 – Hydrogen flow profile (both defined and actual) against vehicle pedal position.

zone thermodynamic model and assuming homogenous conditions and ideal gas behaviour [48]. It is pertinent to repeat here that the reduction in intake O_2 was achieved by aspirating N_2 to simulate EGR-like conditions inside the cylinder. For each intake air boost condition in Fig. 7b, three heat release rate curves are shown, one for the diesel only tests, and the other two representing different H_2 levels (8% and 28%), while maintaining a constant engine load (which was achieved by substituting fossil diesel fuel with H_2).

First considering the ignition delay, it can be observed from Fig. 7a that H_2 substitution increases the ignition delay at both 4 bar and 7 bar IMEP. This could be attributed to the intake air being replaced by H_2 inside the cylinder resulting in reduced O_2 available for mixing with diesel during the ignition delay period. Hence the H_2 could be acting as a diluent, slowing down the low temperature diesel fuel breakdown reactions. However, at higher loads with intake air boosting, no significant change in ignition delay occurs when the H_2 substitution levels are changed (Fig. 7b). This could be because intake air boosting adds a considerable amount of O_2 to the in-cylinder charge, and substitution of air by H_2 (at the levels used for these tests) does not have a significant impact on the fuel breakdown reactions. Similar findings have been reported in Ref. [28], whereby the authors compared H_2-diesel co-combustion in light and heavy duty engines. Fig. 7b also shows that the ignition delay reduces with increasing boost pressure, which could potentially be due to an increase in the intake O_2 concentration, the increased availability of which may accelerate the rate of the low temperature fuel breakdown reactions that occur during the ignition delay period. Furthermore, higher boost pressures result in higher effective compression ratios, leading to an increase in in-cylinder gas pressures and temperatures, and hence reduced ignition delay periods via increased reaction rates [49,50].

Now considering peak heat release rates (pHRRs), it can be observed from both Fig. 7a and b that for the same engine load condition, the pHRR increases with increasing percentage energy from H_2. The increase in pHRR could be attributed to diesel fuel being replaced by a premixed H_2-air mixture. For diesel fuel only tests, post fuel ignition, subsequent combustion relies on the rate of mixing of diesel fuel and air, that is, diffusion-controlled mixing. On the other hand, for H_2–diesel fuel co-combustion tests, the combustion of the premixed H_2-air, along with diesel fuel combustion, results in faster rates of heat release close to engine TDC, and hence higher peak heat release rates. An exception is observed at 4 bar IMEP with 21% H_2 addition (Fig. 7a) where a reduction in pHRR can be observed due to a very long ignition delay period resulting in the peak heat release occurring further away from TDC.

Fig. 8 shows the specific exhaust emissions of NO_x, total particulate mass, CO_2 and unburned total hydrocarbons (THC) for three engine loads – 4, 5.5 and 7 bar IMEP – with the engine running in a naturally aspirated mode. Fig. 9 shows the same emissions, but at the higher loads of 8.5 bar, 10 bar and 11.5 bar, with intake air boosting and a constant 1% reduction in intake O_2. The 1% reduction in intake O_2 condition was selected based on preliminary tests by the authors, whereby it was observed that any decrease in the intake O_2 concentration beyond 1% resulted in an increase in exhaust unburned

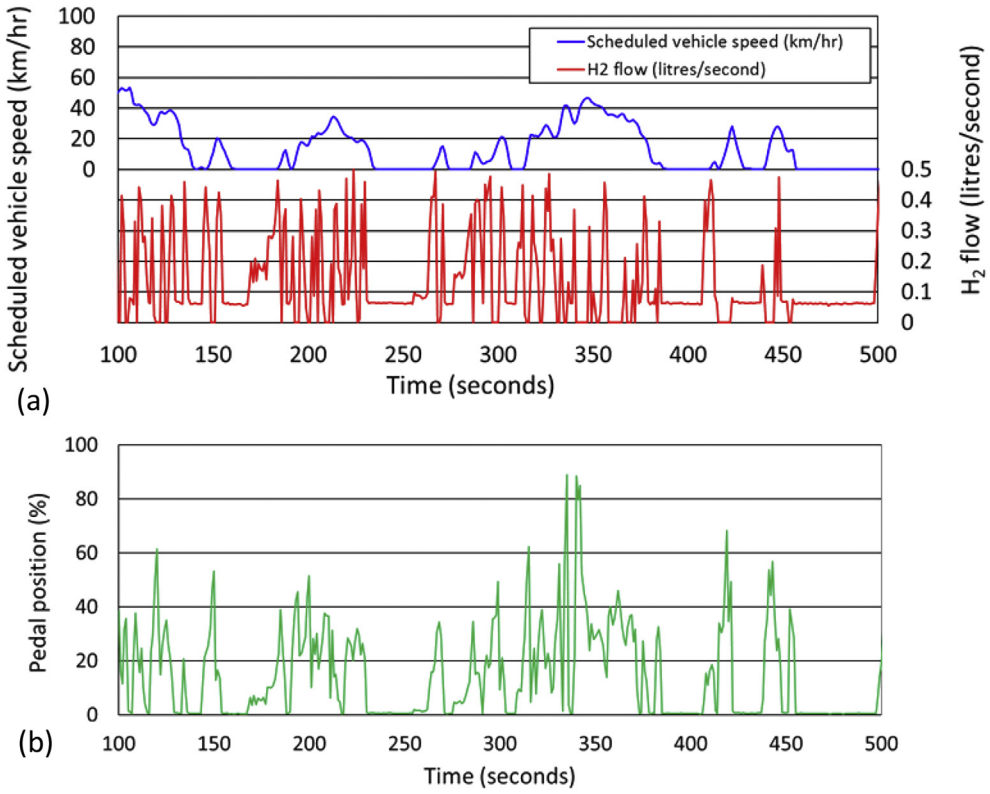

Fig. 6 – (a) Expected H_2 flow (l/min) during part of the PCO-Cenex TfL Taxi drive cycle, (b) pedal position for the same portion of the drive cycle.

hydrocarbon emissions, which is undesirable for any practical combustion application.

First considering NO_x emissions (Fig. 8a), it can be observed that for a load of 4 bar IMEP, NO_x emissions tend to decrease as the percentage energy from H_2 is increased (and diesel fuel energy contribution is reduced). However, for the higher engine load conditions of 5.5 bar and 7 bar, NO_x emissions increase with increasing H_2 energy. Now considering the NO_x results presented in Fig. 9a, it can be observed that at the higher loads conditions, at up to about 10% energy from H_2, there is no significant influence of the presence of H_2 on NO_x levels as the energy contribution from H_2 is increased. However, beyond 10% H_2, exhaust NO_x levels rise considerably as the percentage energy from H_2 is increased. These observations can be explained by considering the conceptual combustion of diesel fuel in a compression ignition engine. Diesel fuel combustion typically occurs at near-stoichiometric conditions, with the resultant temperatures expected to be high enough for significant NO_x production [51]. As diesel fuel is progressively replaced by H_2, the original source of NO_x emissions, i.e. diesel fuel, is substituted by a leaner H_2-air mixture. It follows that at low H_2 levels, this lean H_2-air mixture might not result in sufficiently high local gas temperatures to produce similar levels of NO_x to that of diesel fuel, that the H_2 has substituted and, therefore, the overall NO_x emissions reduce (4 bar IMEP in Fig. 8a) or do not show any considerable increase (for other engine load IMEPs). Beyond 10% energy from H_2, the aspirated H_2-air mixture becomes less lean, and H_2 addition appears to result in higher peak heat release rates (as can be seen in Fig. 7), thereby increasing local temperatures, and increasing thermal NOx production. The same explanation holds true for the increase in NO_x emissions observed at engine loads of 5.5 bar and 7 bar IMEP with the engine running in its naturally aspirated condition. The effect of local temperatures has been previously observed [20] whereby the H_2 flame temperatures correlated well with the threshold temperature for significant NO_x production.

Considering the exhaust emissions of the total particulate mass (TPM), considerable reductions in TPM levels were observed at all 3 engine loads for the naturally aspirated tests (Fig. 8b). Furthermore, a significant reduction in TPM can be observed at the lowest intake air boost condition of 1.33 bar, whereby TPM emissions exhibit a reduction of about 50% at 10% energy from H_2 relative to diesel-only combustion (Fig. 9b). This reduction can be attributed to the replacement of diesel fuel with H_2, which does not produce any carbon-based emissions on combustion. However, similar reductions in TPM levels are not observed in the case of the other two intake air boost-engine load conditions.

Considering Figs. 8c and 9c, CO_2 emissions are observed to decrease as the percentage energy contribution from H_2 is progressively increased and a linear reduction in CO_2 emissions is expected as diesel fuel is substituted by H_2. However, it is interesting to note that at higher levels of percentage energy from H_2 (above 25%), the reduction in CO_2 emissions is greater than what can be expected from simple fuel carbon displacement. This could be due to the aspirated H_2 displacing the intake air and reducing the amount of O_2 available for the oxidation of diesel fuel, especially at the higher H_2 flow rates (or higher levels of percentage energy

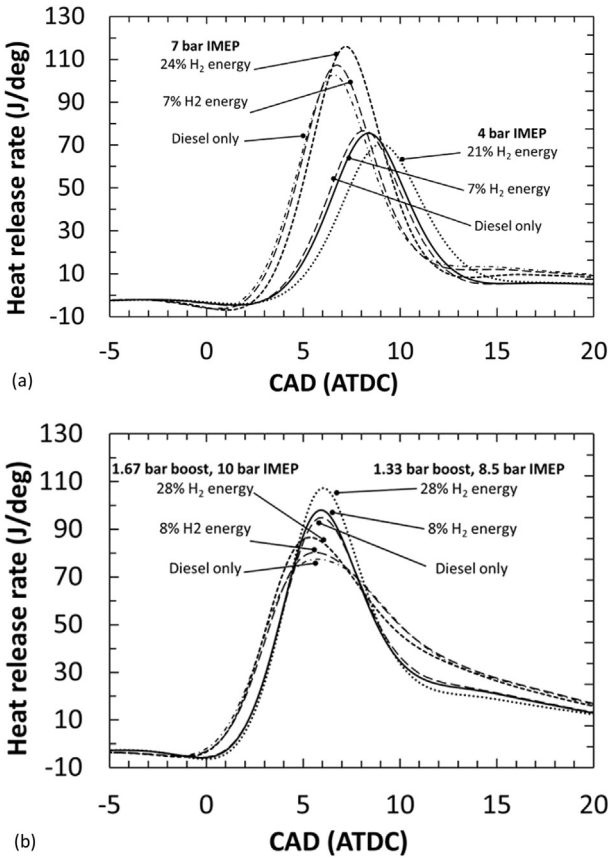

Fig. 7 – Apparent net heat release rate curves with varying energy (%) from H_2 at (a) lower load conditions and (b) higher load conditions with intake air boosting and a constant intake O_2 reduction level of 1%.

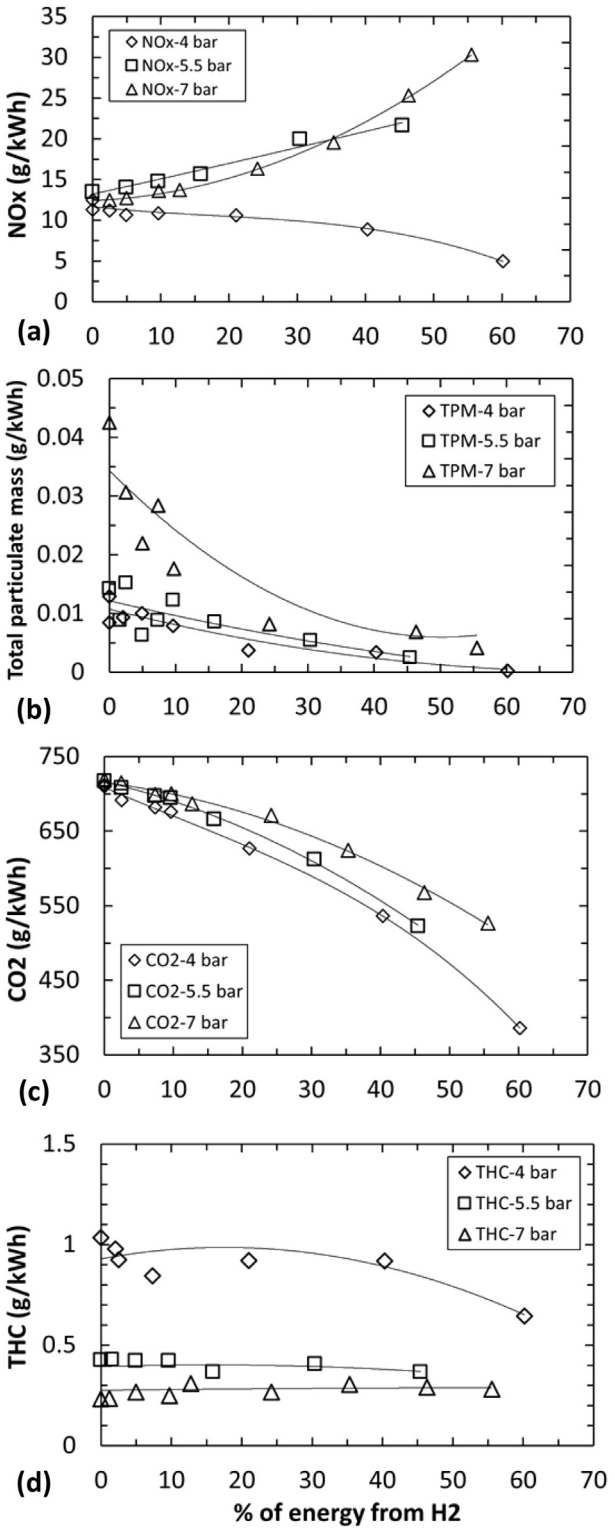

Fig. 8 – Specific emissions of (a) NO_x, (b) total particulate mass, (c) CO_2 and (d) unburned total hydrocarbons (THC) for different engine loads and varying % energy from H_2, with the engine running in a naturally aspirated mode.

from H_2), and hence resulting in less CO_2 being formed (and effectively reducing the combustion efficiency of the fossil diesel). The exhaust emissions of unburned total hydrocarbons (THC) in Fig. 9d exhibit a slight increase at the higher H_2 energy levels, can similarly be attributed to a reduction in O_2 available for carbon oxidation, due to displacement by the aspirated H_2.

Fig. 10 shows the total number of particles in the engine exhaust gas for the three intake air pressure-engine load combinations, a constant 1% reduction in intake O_2 and varying percentage energy from H_2. (It should be noted that the measurement range of the equipment used to measure particle size and number on the single cylinder engine at UCL is different from the one use used to measure particle number on the vehicle at Horiba-MIRA. The equipment used on the vehicle is specified to measure 90% of the particulate number at 41 nm and 50% at 23 nm. A roll-off 'filter' profile was created by MIRA and supplied to UCL for their analysis work. This filter was applied on the data obtained by UCL, to allow reliable comparison between the two sets of data, and has been presented in Fig. 10.) The number of particles in the engine exhaust increased when the engine load is increased. This is to be expected, as at higher engine loads the diesel fuel injection duration is significantly longer and thus the tail-end of the fuel injection occurs after the start of combustion [48,52]. Thus, the injected fuel has less opportunity to mix with the intake air, leading to a greater amount of diffusion rate controlled combustion (Fig. 7) and a longer duration of conditions suited to pyrolysis and particle formation. Considering the effect of H_2

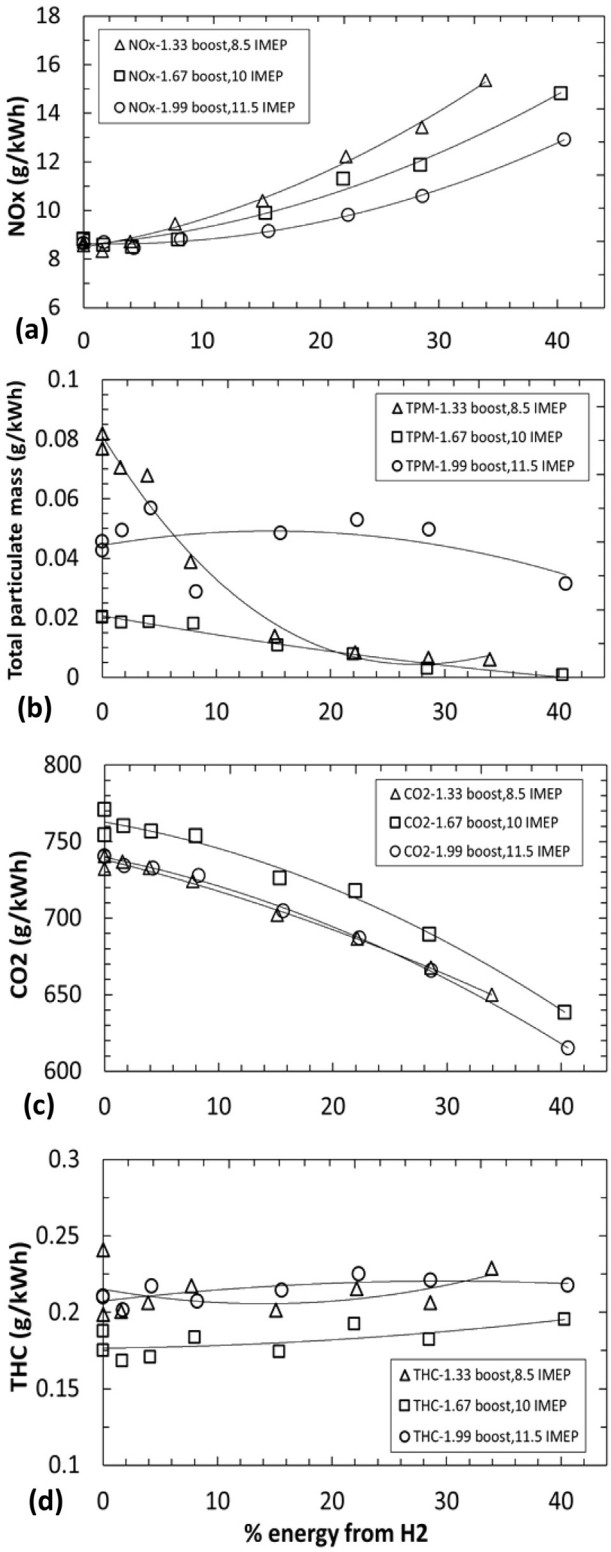

Fig. 9 – Specific emissions of (a) NO_x, (b) total particulate mass, (c) CO_2 and (d) unburned total hydrocarbons (THC) for different intake air pressure - engine load conditions and varying % energy from H_2, at a constant 1% reduction in intake O_2.

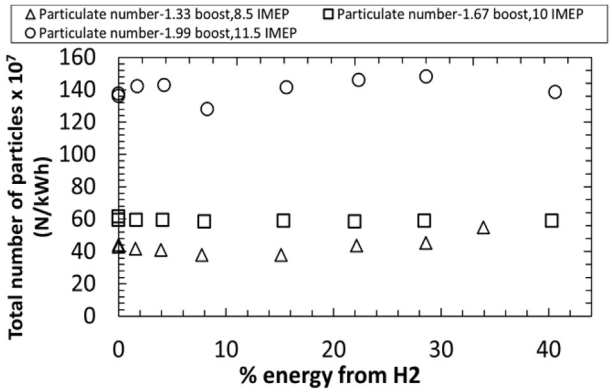

Fig. 10 – Total particulate number emissions (N/kWh) for different intake air pressure - engine load conditions and varying % energy from H_2, at a constant 1% reduction in intake O_2.

on the number of particles in the engine exhaust, no significant effect can be observed from Fig. 10, except for a slight increase in the number of particles for the lowest intake air pressure-engine load condition of 1.33 bar boost and 8.5 bar IMEP. This could potentially be attributed to a reduction in intake O_2 due to displacement by the aspirated H_2, as discussed earlier. This effect is not apparent at the higher intake air boost conditions probably due to an increase in the effective compression ratio, which would enhance the rate of carbon oxidation.

Fig. 11 shows the size distribution of the number of particles in the engine exhaust gas at varying percentage energy from H_2, intake air pressure of 1.33 bar, engine load of 8.5 bar IMEP and a reduction in intake O_2 of 1%. To avoid repetition, the size distribution graphs for the other test conditions are not shown as they show largely similar trends. A reduction in the number of particles is observed in Fig. 11 when the percentage energy from H_2 is increased. This reduction occurs primarily for particles of diameters ranging between 0.05 μm and 0.2 μm, which are typically classified as fine (Dp < 2.5 μm, PM2.5) and ultrafine (Dp < 0.1 μm) particles [53].

Fig. 12 shows the indicated thermal efficiency for different engine operating conditions and varying levels of H_2 addition, with the engine running in naturally aspirated mode (Fig. 12a) and with 1% reduction in intake O_2 and intake air boosting (Fig. 12b). The indicated thermal efficiency was calculated as the ratio of the engine output power to the combined calorific input from both diesel fuel and hydrogen. It should be noted that since the intake air was being boosted by a supercharger, some work was being added to the engine cycle via the boosting process, and this is reflected in the higher indicated thermal efficiencies presented in Fig. 12b. Overall it can be observed that the indicated thermal efficiency reduces with increasing H_2 addition. This is consistent with the results of CO_2 emissions observed in Figs. 8c and 9c, which also showed a reduction with H_2 addition. It is believed that the observed reduction in thermal efficiency with increasing H_2 addition is due to a proportion of the aspirated H_2 not taking part in the combustion process and being exhausted from the engine

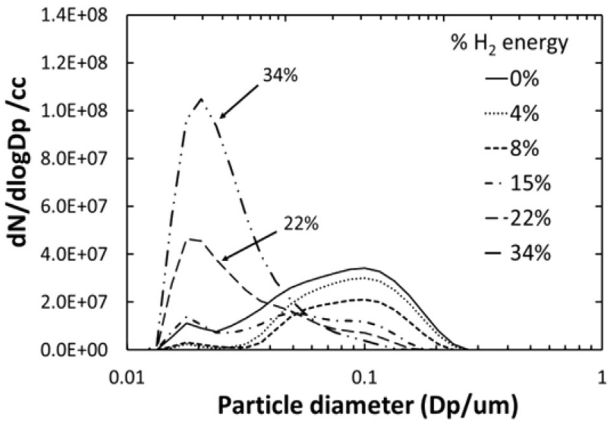

Fig. 11 – Particulate number distribution for 1.33 bar intake air pressure – 8.5 bar IMEP engine load, at varying percentage energy from H_2 and a constant 1% reduction in intake O_2.

unburned. As the amount of H_2 in the exhaust was not measured, it could not be accounted for when calculating the indicated thermal efficiencies.

Chassis dynamometer vehicle drive cycle tests

Fig. 13 shows the exhaust emissions of CO, CO_2 and NO_x, while Fig. 14 shows the exhaust emissions of particulate mass and the number of particles for both the diesel only and the H_2-diesel co-combustion tests, conducted on the demonstration vehicle. The results for these tests showing the emission levels from each stage of the test have been tabulated and presented in Appendix.

First considering Fig. 13, CO and CO_2 exhibit a reduction of about 13% and 5% respectively, when H_2 is added, which could be attributed to the carbon-containing diesel being substituted by H_2 at approximately 10% by energy at low engine loads, dependent on the accelerator pedal position (Fig. 5). NO_x emissions also show a reduction of approximately 11% when H_2 is added to the engine. The reduction in NO_x was also observed at the low load condition of 4 bar IMEP in the single cylinder engine tests, and can therefore be similarly attributed to the replacement of some of the diesel fuel with a much leaner H_2-air mixture. This would result in an overall reduction in in-cylinder gas temperatures, and hence a decrease in NO_x formation rates. Some preliminary analysis of the drive cycle used in these experiments showed that the vehicle operated at a range of engine power between 1 kW and 7 kW for most part of the cycle (Fig. 15), which is similar to the loads used for the single cylinder tests. Hence, a similar behaviour of NO_x emissions is likely to be expected.

Another potential reason for this reduction in NO_x could be likely higher EGR flow rates when H_2 is added to the engine. The addition of H_2 to the in-cylinder charge would cause the torque output, and hence the engine speed, to increase. In turn, the vehicle operator will have to lift off the accelerator pedal in order to reduce the engine speed to the prescribed speed of the drive cycle. This could result in an increase in EGR flow rates, since EGR rates are higher at lower engine loads, and hence reduced NO_x emissions (and potentially increased particulate emissions – Fig. 14a). There is some evidence for this in the test data shown in Fig. 6, where the pedal position seems to correlate well with the H_2 flow to the engine throughout the drive cycle. The addition of H_2 could also affect the response of the exhaust lambda sensor, in that, due to the displacement of intake air by H_2, the exhaust lambda sensor would detect lower levels of O_2 than is expected for a certain engine load. This could lead to the ECU to reduce diesel fuel injection in order to optimise the in-cylinder mixture for maximum power output.

Now considering Fig. 14, the particulate mass emissions increased by 24% when H_2 was added, however the number of particles reduced by 5.5% with H_2 augmentation. The increase in particulate mass could be attributed to a reduction in O_2 available inside the combustion chamber for carbon oxidation, as a result of the displacement of intake air by the aspirated H_2, as well as increased rates of EGR (as discussed earlier) due to H_2 being added to the engine. The reduction in particle number could potentially imply the production of more of the larger or agglomerated particles, and perhaps less of the smaller ones that lie in the fine and ultrafine range of sizes. This reduction was also observed in the single cylinder tests (Fig. 11), where the number of particles with diameters between 0.05 μm and 0.2 μm, reduced when the percentage energy from H_2 was increased. It is interesting to note that while particulate mass increased, CO and CO_2 emissions reduced, with increasing H_2 addition. It could be speculated that this is due to particulates having comparatively smaller

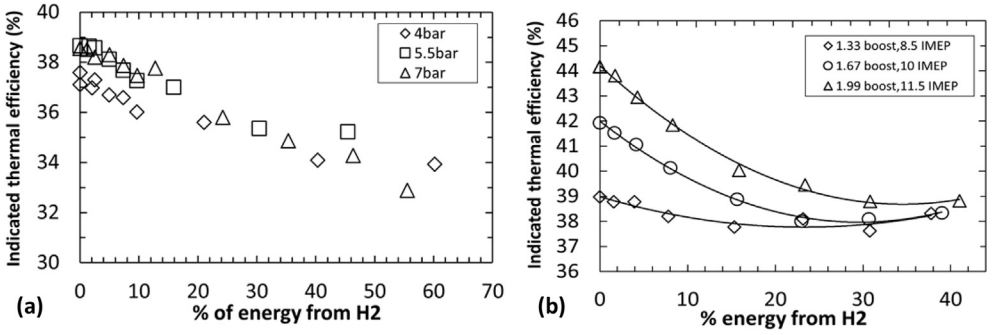

Fig. 12 – Indicated thermal efficiency for different engine loads and varying % energy from H_2, with the engine running in (a) naturally aspirated mode and (b) at a constant 1% reduction in intake O_2 with different intake air boost.

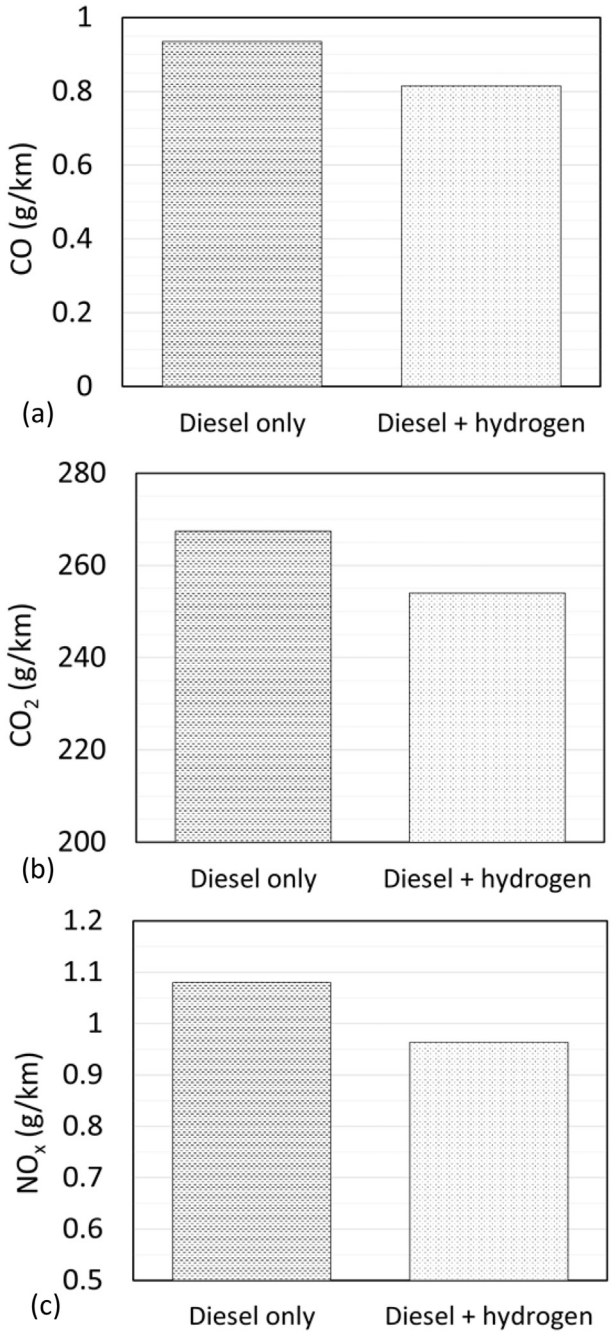

Fig. 13 – Exhaust emissions of (a) CO, (b) CO_2 and (c) NO_x from the demonstration vehicle, for both diesel only and H_2-diesel co-combustion tests.

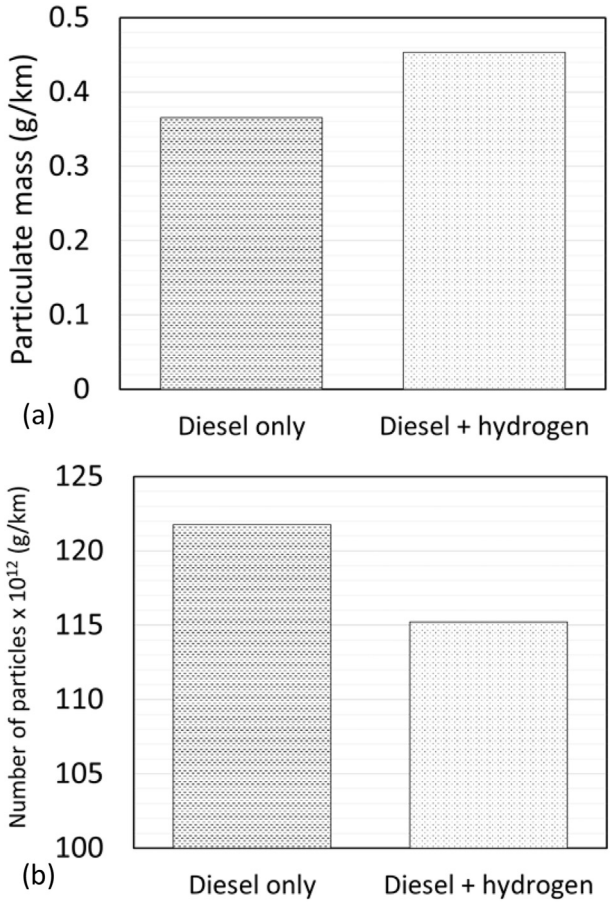

Fig. 14 – Exhaust emissions of (a) particulate mass and (b) number of particles from the demonstration vehicle, for both diesel only and H_2-diesel co-combustion tests.

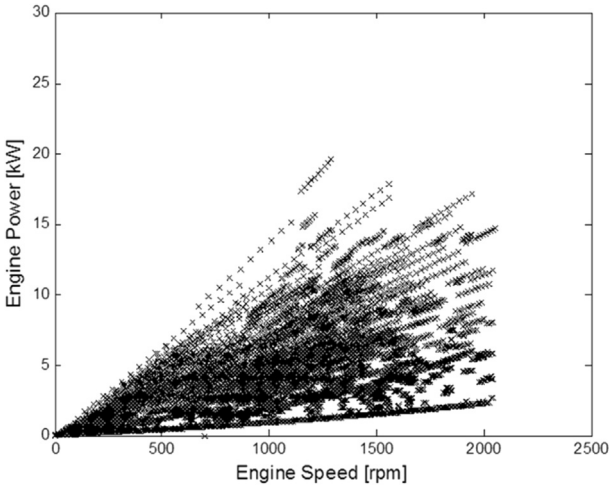

Fig. 15 – Engine power and engine speed data points for the chassis vehicle tests.

quench limits, and hence are impacted more by the reduction on oxygen content, relative to CO and CO_2.

Potential of low level H_2 addition for improving emissions performance

Based on the work conducted in this study whereby H_2-diesel co-combustion tests were carried out on a single cylinder engine and in a test vehicle, it could be suggested that the use of H_2 would be favourable below a level of approximately 10% energy from H_2, where a reduction in CO and CO_2 emission was observed, and the NO_x emissions either did not change or exhibited a reduction, depending on the engine running parameters. In the case of particle number, both test facilities showed a reduction in the number of particles, but the test

vehicle showed a considerable increase in particulate mass, which implied the production of larger sized particles. It is possible that these larger particles would be captured in a DPF (diesel particulate filter), not fitted to this test vehicle for these tests, and therefore an overall reduction in both particulate mass and particle number could potentially be achieved. For any practical application, the hydrogen augmentation system would need to be tested and integrated with other emission reduction measures employed in vehicles such as after treatment systems (SCR, EGR, etc.). Additionally, it could also be suggested that since the supply of on-board H_2 available for use with such aftermarket retro-fit solutions is likely to be limited in volume, and H_2 does not offer any benefits at high levels of addition (for example, NO_x emissions increase at high H_2 addition levels), the use of H_2 could be limited to transient stages of the drive cycle, for example, when the vehicle starts to move from a complete stop. Under these circumstances, the engine is relatively cold, and diesel fuel that is injected tends to pyrolyse more easily to form particulates and therefore the part substitution of diesel fuel with H_2 at these specific transients could potentially result in substantial reductions in exhaust particulate emissions.

Conclusions

The following conclusions can be drawn from the single cylinder engine tests:

1. The peak heat release rates increased with increasing percentage energy from H_2, attributable to H_2 ignition resulting in faster rates of heat release closer to engine TDC position.
2. Exhaust NO_x emissions reduced at low engine load conditions with H_2 substitution, and increased only when the energy from H_2 was increased beyond 8–10%, which was attributed to the H_2 resulting in local hotspots, thereby increasing thermal NO_x production.
3. The number of particles, with diameters ranging between 0.05 and 0.2 μm, reduced with increasing percentage energy from H_2.

The following outcomes can be summarised from the vehicle demonstration tests:

1. 10% hydrogen augmentation in the vehicle reduced the exhaust emissions of CO, CO_2 and NO_x by 13%, 5% and 11% respectively, during the overall drive cycle.
2. An increase in the particulate mass, but a reduction in the total number of particles was observed when H_2 was added.

Acknowledgements

The authors would like to acknowledge Innovate UK (Project No. 101583) for their financial contribution to this project, and both Cella Energy Ltd. and Productiv Group for support of this work.

Appendix

The results of the exhaust emissions from the demonstration vehicle drive cycle tests, for both the diesel only experiments and those utilising the H_2-diesel fuel co-combustion, have been summarised in Table A. The tests were divided into 4 phases due the capacity of the sampling bag used for collecting the gaseous emissions, with the table showing the measured emission concentration for each phase and also the total masses recorded over the entirety of the drive cycle.

Table A – Exhaust emission results from (a) diesel only and (b) H_2-diesel fuel co-combustion tests carried out for a complete drive cycle on the demonstration vehicle.

	CO	CO_2	THC	NO_x	PM	Particle No.	
(a) Diesel only							
Phase 1 g	7.338	1151.4	1.882	4.694	0.556	5.191E+14	#
Phase 1 g/km	2.112	331.4	0.542	1.351		1.494E+14	#/km
Phase 2 g	2.394	861.4	0.444	3.369	1.057	4.177E+14	#
Phase 2 g/km	0.796	286.4	0.148	1.120		1.389E+14	#/km
Phase 3 g	1.591	712.6	0.187	2.933	1.118	3.052E+14	#
Phase 3 g/km	0.565	253.0	0.066	1.041		1.083E+14	#/km
Phase 4 g	1.084	825.3	0.155	3.345	2.119	3.746E+14	#
Phase 4 g/km	0.272	207.272	0.039	0.840		9.407E+13	#/km
Total Mass g	12.407	3550.7	2.667	14.341	4.850	1.617E+15	#
Total Mass g/km	0.934	267.4	0.201	1.080	0.365	1.218E+14	#/km
(b) Diesel + Hydrogen							
Phase 1 g	7.257	1050.5	1.957	3.889	0.710	4.850E+14	#
Phase 1 g/km	2.096	303.4	0.565	1.123		1.401E+14	#/km
Phase 2 g	1.652	817.7	0.287	3.005	1.377	3.887E+14	#
Phase 2 g/km	0.550	272.3	0.096	1.001		1.294E+14	#/km
Phase 3 g	1.200	698.5	0.170	2.808	1.355	2.979E+14	#
Phase 3 g/km	0.428	249.0	0.061	1.001		1.062E+14	#/km
Phase 4 g	0.694	800.7	0.145	3.067	2.567	3.728E+14	#
Phase 4 g/km	0.174	200.889	0.036	0.769		9.353E+13	#/km
Total Mass g	10.802	3367.5	2.558	12.769	6.009	1.528E+15	#
Total Mass g/km	0.815	254.0	0.193	0.963	0.453	1.152E+14	#/km

Nomenclature

ATDC	after-top-dead-centre
BTDC	before-top-dead-centre
CAD	crank angle degree
CI	compression ignition
CO	carbon monoxide
CO_2	carbon dioxide
Dp	particle diameter
EGR	exhaust gas recirculation
H_2	hydrogen
IMEP	indicated mean effective pressures
NO_x	nitrogen oxides
O_2	oxygen
PM	particulate mass
rpm	revolutions per minute
SCR	selective catalyst reduction
SOC	start of combustion
SOI	start of injection
TDC	top-dead-centre
THC	total hydrocarbons

REFERENCES

[1] European Parliament and Council. Euro 5 and Euro 6 standards: reduction of pollutant emissions from light vehicles 2010.

[2] COMEAP. The mortality effects of long-term exposure to particulate air pollution in the United Kingdom. 2010.

[3] Walton H, Dajnak D, Beevers S, Williams M, Watkiss P, Hunt A. Understanding the health impacts of air pollution in London. 2015.

[4] Viewpoint: The trouble with diesel - BBC News n.d. http://www.bbc.co.uk/news/science-environment-38814297 (accessed February 2, 2017).

[5] Wang T, Jerrett M, Sinsheimer P, Zhu Y. Estimating PM2.5-associated mortality increase in California due to the Volkswagen emission control defeat device. Atmos Environ 2016;144:168–74. https://doi.org/10.1016/j.atmosenv.2016.08.074.

[6] C40 Cities. C40 blog - daring cities make bold air quality commitment to remove all diesel vehicles by 2025. 2016. http://www.c40.org/blog_posts/daring-cities-make-bold-air-quality-commitment-to-remove-all-diesel-vehicles-by-2025. [Accessed 2 February 2017].

[7] Zimmerman N. Move is on to ban diesel cars from cities | Business| Economy and finance news from a German perspective. WwwDwCom; 2018. DW | 26.02.2018.

[8] SMMT. UK new car market declines in 2017 but demand still third highest in 10 years. SMMT; 2018.

[9] Johnson TV. Review of diesel emissions and control. Int J Engine Res 2009;10:275–85. https://doi.org/10.1243/14680874JER04009.

[10] Guan B, Zhan R, Lin H, Huang Z. Review of state of the art technologies of selective catalytic reduction of NO_x from diesel engine exhaust. Appl Therm Eng 2014;66:395–414. https://doi.org/10.1016/j.applthermaleng.2014.02.021.

[11] Transport for London. Ultra Low Emission Zone - Transport for London n.d. https://tfl.gov.uk/modes/driving/ultra-low-emission-zone (accessed February 4, 2017).

[12] Zhou JH, Cheung CS, Leung CW. Combustion, performance and emissions of a diesel engine with H_2, CH_4 and H_2–CH_4 addition. Int J Hydrogen Energy 2014;39:4611–21. https://doi.org/10.1016/j.ijhydene.2013.12.194.

[13] Tira HS, Herreros JM, Tsolakis A, Wyszynski ML. Influence of the addition of LPG-reformate and H_2 on an engine dually fuelled with LPG–diesel, –RME and –GTL Fuels. Fuel 2014;118:73–82.

[14] Thangaraj S, Govindan N. Investigating the pros and cons of browns gas and varying EGR on combustion, performance, and emission characteristics of diesel engine. Environ Sci Pollut Res 2018;25:422–35. https://doi.org/10.1007/s11356-017-0369-4.

[15] Tüccar G. Effect of hydroxy gas enrichment on vibration, noise and combustion characteristics of a diesel engine fueled with Foeniculum vulgare oil biodiesel and diesel fuel. Energy Sources Part A Recover Util Environ Eff 2018;40:1257–65. https://doi.org/10.1080/15567036.2018.1476622.

[16] Jamrozik A, Tutak W, Pyrc M, Gruca M, Kočiško M. Study on co-combustion of diesel fuel with oxygenated alcohols in a compression ignition dual-fuel engine. Fuel 2018;221:329–45. https://doi.org/10.1016/J.FUEL.2018.02.098.

[17] Sahoo BB, Sahoo N, Saha UK. Effect of engine parameters and type of gaseous fuel on the performance of dual-fuel gas diesel engines—a critical review. Renew Sustain Energy Rev 2009;13:1151–84. https://doi.org/10.1016/j.rser.2008.08.003.

[18] Wagemakers AMLM, Leermakers CAJ. Review on the effects of dual-fuel operation, using diesel and gaseous fuels, on emissions and performance. 2012. https://doi.org/10.4271/2012-01-0869.

[19] Saravanan N, Nagarajan G, Sanjay G, Dhanasekaran C, Kalaiselvan KM. Combustion analysis on a DI diesel engine with hydrogen in dual fuel mode. Fuel 2008;87:3591–9.

[20] Talibi M, Hellier P, Balachandran R, Ladommatos N. Effect of hydrogen-diesel fuel co-combustion on exhaust emissions with verification using an in–cylinder gas sampling technique. Int J Hydrogen Energy 2014;39:15088–102. https://doi.org/10.1016/j.ijhydene.2014.07.039.

[21] Tüccar G, Uludamar E. Emission and engine performance analysis of a diesel engine using hydrogen enriched pomegranate seed oil biodiesel. Int J Hydrogen Energy 2018;43:18014–9. https://doi.org/10.1016/J.IJHYDENE.2017.11.124.

[22] Akar MA, Kekilli E, Bas O, Yildizhan S. Hydrogen enriched waste oil biodiesel usage in compression ignition engine. Int J Hydrogen Energy 2018;43:18046–52. https://doi.org/10.1016/J.IJHYDENE.2018.02.045.

[23] Yıldızhan Ş. Hydrogen addition to tea seed oil biodiesel: performance and emission characteristics. Int J Hydrogen Energy 2018;43:18020–7. https://doi.org/10.1016/J.IJHYDENE.2017.12.085.

[24] Chaichan MT. Performance and emission characteristics of CIE using hydrogen, biodiesel, and massive EGR. Int J Hydrogen Energy 2018;43:5415–35. https://doi.org/10.1016/j.ijhydene.2017.09.072.

[25] Morgan R, Heikal M, Atkins AF, Atkins P. Results from the testing of a heavy duty diesel engine with hydrogen fumigation. 2016.

[26] Jhang S-R, Chen K-S, Lin S-L, Lin Y-C, Cheng WL. Reducing pollutant emissions from a heavy-duty diesel engine by using hydrogen additions. Fuel 2016;172:89–95. https://doi.org/10.1016/j.fuel.2016.01.032.

[27] Gatts T, Li H, Liew C, Liu S, Spencer T, Wayne S, et al. An experimental investigation of H_2 emissions of a 2004 heavy-duty diesel engine supplemented with H_2. Int J Hydrogen Energy 2010;35:11349–56. https://doi.org/10.1016/j.ijhydene.2010.06.056.

[28] Talibi M, Hellier P, Morgan R, Lenartowicz C, Ladommatos N. Hydrogen-diesel fuel co-combustion strategies in light duty and heavy duty CI engines. Int J Hydrogen Energy

2018;43:9046–58. https://doi.org/10.1016/j.ijhydene.2018.03.176.
[29] Koten H. Hydrogen effects on the diesel engine performance and emissions. Int J Hydrogen Energy 2018;43:10511–9. https://doi.org/10.1016/J.IJHYDENE.2018.04.146.
[30] Morgan R, Atkins P, Atkins A, Lenartowicz C, Heikal M. Effect of hydrogen fumigation in a dual fueled heavy duty engine. SAE Tech. Pap. 2015. https://doi.org/10.4271/2015-24-2457.
[31] Tsolakis A, Megaritis A. Catalytic exhaust gas fuel reforming for diesel engines—effects of water addition on hydrogen production and fuel conversion efficiency. Int J Hydrogen Energy 2004;29:1409–19.
[32] BERNAUER O. Development of hydrogen-hydride technology in the F.R.G. Int J Hydrogen Energy 1989;14:727–35. https://doi.org/10.1016/0360-3199(89)90089-X.
[33] DAS L. Hydrogen engines: a view of the past and a look into the future. Int J Hydrogen Energy 1990;15:425–43. https://doi.org/10.1016/0360-3199(90)90200-I.
[34] Nathanson AS, Ploszajski AR, Billing M, Cook JP, Jenkins DWK, Headen TF, et al. Ammonia borane–polyethylene oxide composite materials for solid hydrogen storage. J Mater Chem A 2015;3:3683–91. https://doi.org/10.1039/C4TA06657J.
[35] Mazzucco A, Dornheim M, Sloth M, Jensen TR, Jensen JO, Rokni M. Bed geometries, fueling strategies and optimization of heat exchanger designs in metal hydride storage systems for automotive applications: a review. Int J Hydrogen Energy 2014;39:17054–74. https://doi.org/10.1016/J.IJHYDENE.2014.08.047.
[36] Hellier P, Ladommatos N, Headen T, Bennington S. Engine testing of dissolved sodium borohydride for diesel combustion CO_2 scrubbing. SAE Tech Pap 2014; 2014–Octob. https://doi.org/10.4271/2014-01-2729.
[37] Engineering - Cella Energy n.d. http://cellaenergy.com/engineering (accessed April 4, 2017).
[38] Lilik GK, Zhang H, Herreros JM, Haworth DC, Boehman AL. Hydrogen assisted diesel combustion. Int J Hydrogen Energy 2010;35:4382–98.
[39] Masood M, Ishrat MM, Reddy AS. Computational combustion and emission analysis of hydrogen–diesel blends with experimental verification. Int J Hydrogen Energy 2007;32:2539–47.
[40] Saravanan N, Nagarajan G. An experimental investigation of hydrogen-enriched air induction in a diesel engine system. Int J Hydrogen Energy 2008;33:1769–75. https://doi.org/10.1016/j.ijhydene.2007.12.065.
[41] Shin B, Cho Y, Han D, Song S, Chun KM. Hydrogen effects on NO_x emissions and brake thermal efficiency in a diesel engine under low-temperature and heavy-EGR conditions. Int J Hydrogen Energy 2011;36:6281–91. https://doi.org/10.1016/j.ijhydene.2011.02.059.
[42] Talibi M, Hellier P, Ladommatos N. The effect of varying EGR and intake air boost on hydrogen-diesel co-combustion in CI engines. Int J Hydrogen Energy 2016. https://doi.org/10.1016/j.ijhydene.2016.11.207.
[43] Banerjee R, Roy S, Bose PK. Hydrogen-EGR synergy as a promising pathway to meet the PM–NO_x–BSFC trade-off contingencies of the diesel engine: a comprehensive review. Int J Hydrogen Energy 2015;40:12824–47. https://doi.org/10.1016/j.ijhydene.2015.07.098.
[44] Roy MM, Tomita E, Kawahara N, Harada Y, Sakane A. An experimental investigation on engine performance and emissions of a supercharged H2-diesel dual-fuel engine. Int J Hydrogen Energy 2010;35:844–53. https://doi.org/10.1016/j.ijhydene.2009.11.009.
[45] Dimitriou P, Kumar M, Tsujimura T, Suzuki Y. Combustion and emission characteristics of a hydrogen-diesel dual-fuel engine. Int J Hydrogen Energy 2018;43:13605–17. https://doi.org/10.1016/J.IJHYDENE.2018.05.062.
[46] Talibi M, Hellier P, Balachandran R, Ladommatos N. Development of a fast-acting, time-resolved gas sampling system for combustion and fuels analysis. SAE Int J Engines 2016;9(2):1102–16. https://doi.org/10.4271/2016-01-0791. 2016-2101–0791.
[47] Saravanan N, Nagarajan G, Sanjay G, Dhanasekaran C, Kalaiselvan KM. Combustion analysis on a DI diesel engine with hydrogen in dual fuel mode. Fuel 2008;87:3591–9. https://doi.org/10.1016/j.fuel.2008.07.011.
[48] Heywood JB. Internal combustion engine fundamentals, vol. 21; 1988.
[49] Westbrook CK. Chemical kinetics of hydrocarbon ignition in practical combustion systems. Proc Combust Inst 2000;28:1563–77. https://doi.org/10.1016/S0082-0784(00)80554-8.
[50] Thoo WJ, Kevric A, Ng HK, Gan S, Shayler P, La Rocca A. Characterisation of ignition delay period for a compression ignition engine operating on blended mixtures of diesel and gasoline. Appl Therm Eng 2014;66:55–64. https://doi.org/10.1016/j.applthermaleng.2014.01.066.
[51] Dec JEA. Conceptual model of DI diesel combustion based on laser-sheet imaging. SAE Pap; 1997. p. 970873. https://doi.org/10.4271/970873.
[52] Stone R. Introduction to internal combustion engines. 4th ed. New York: Palgrave Macmillan Limited; 2012.
[53] Kittelson D, Watts W, Johnson J. Diesel aerosol sampling methodology. Minneapolis, USA: CRC E-43; 2002.